Experiments in Fluids 28 (2000) 11–20 © Springer-Verlag 2000

Helical-mode excitation of lifted flames using piezoelectric actuators

Y.-C. Chao, Y.-C. Jong, H.-W. Sheu

Abstract Experiments of helical excitation using piezoelectric actuators on jet flows and lifted flames are performed to enhance the understanding of the effects of vortical structures of various instability modes on the stabilization mechanism of the lifted flame. In addition to the common ring and braid structures, five or seven azimuthal fingers (or lobes) can be identified in the transverse image of the jet near field. Excitation with various helical modes enhances the azimuthal structures and entrainment in the near field. When helically excited with the asymmetric $m=1$ mode, one of the fingers is enhanced and may evolve into a strong streamwise vortex. The streamwise vortices generated in the braid region between the adjacent ring vortices may enhance fuel-air mixing due to additional azimuthal entrainment upstream of a lifted flame when helically excited with the $m=1$ mode. Therefore, the streamwise vortex serves as an additional path of high probability of premixed flammable layer for the upstream propagation of the lifted flame so that the flame base on one side of the lifted flame may extend farther upstream and the flame base is inclined. In addition to the inclined flame base, multiple-legs phenomenon is also observed in the flame base, which is strongly associated with fingers of the helical modes of the jet flow.

1 Introduction

For decades, the existence of large scale coherent structures in the near field of jet flows has already been confirmed and studied by an overwhelming number of investigations, see review by Ho and Huerre (1984). The near field of turbulent jet flow is dominated by large-scale coherent structures which play a key role in transports of heat, mass and momentum, aerodynamic noise generation, effluent mixing for cooling, chemical reaction and dilution of chemical systems, etc. Only until recent years did the dynamic stabilization behavior of a lifted jet flame receive extensive attention. The stability phenomena of lift-off and blowout of a jet flame are usually found in high velocity jet flows. The hysteresis phenomenon of reattaching a lifted flame by reducing the jet flow velocity can only occur when the velocity is reduced to a value well below its original liftoff velocity. The importance of large scale structures on the dynamic behavior of flame stability, and the response of flames to external acoustic excitation were carefully investigated, see Broadwell et al. (1984), Gollahalli et al. (1986), Chao and Jeng (1992), Pitts (1990), and Schefer et al. (1994a). Various models and physical mechanisms have been proposed to delineate the liftoff behavior. Evolution of current liftoff theories has come a long way from the early premixed combustion model of Vanquickenborn and van Tigglen (1996), the flamelet extinction model of Peters and Williams (1983), the large-scale mixing model of Broadwell et al. (1984), the combined premixed flame propagation and flamelet extinction model of Miake-Lye and Hammer (1988) and others, to the recent triple flame model of Müller et al. (1994) and Muñiz and Mungal (1997). Kioni et al. (1993) demonstrated experimentally the stabilization of a stationary triple flame in a burner with well-defined linear concentration gradients. They also showed numerically the propagation of the triple flame for a wide range of strain rates. The structure of the triple flame is composed of a curved rich premixed flame on the fuel side, a curved lean premixed flame on the air side and a long, thin trailing diffusion flame. Ruetsch et al. (1995), by taking account for heat release, depicted in their numerical simulation that flame can be stabilized in a flow with velocity greater than the laminar flame speed. Muñiz and Mungal (1997) measured the instantaneous, two-dimensional velocity field by using PIV (particle image velocimetry). They showed that the fluid velocity conditioned on the instantaneous flame base location is low and close to the laminar flame speed, less than three times of the laminar flow speed, and the velocity profiles at the flame base are similar to those predicted by simulations of triple flames. Everest et al. (1996) used a planar Rayleigh scattering system to visualize the flammable layer and calculate the scalar dissipation rate upstream of the mean flame base location of a lifted nonpremixed jet flame. They showed that regions of low scalar dissipation allow the possibility of upstream flame propagation. Similar concepts of flammable layer and low, close to laminar, instantaneous flame speed at the flame base were used to delineate the near-field stabilization mechanism of a lifted jet flame in the hysteresis region by

Received: *21 August 1997*/*Accepted*: *24 January 1999*

Y.-C. Chao, Y.-C. Jong, H.-W. Sheu
Institute of Aeronautics and Astronautics, National Cheng Kung University, Tainan, Taiwan, 701, R.O.C

Correspondence to: Y.-C. Chao

The financial support by the National Science Council with projects NSC 83-0401-E006-009 and NSC 85-2212-E006-050 is sincerely acknowledged

Chao and Jeng (1992) and Lin et al. (1993) based upon their phase-averaged LDV and gas concentration measurements. In initial phases of a flame-oscillation cycle the propagation of a lifted jet flame along the peripheral flammable layer in the near field of the jet is shown to be retarded due to the large velocity of cold entrainment as a result of major evolutional processes of large-scale vortices such as pairing and rollup. Then, in latter phases of the cycle, the "braid" extending from the trailing edge of the paired vortex to the next up-coming vortex provides a convenient passage with flammable premixture and low velocity for the retarded flame to propagate to the next vortex. For the most part in the past, attentions were confined to the interaction of large-scale vortices of the axisymmetric mode of the jet flow with the flame. However, flow and flame visualization images, as shown in Fig. 4 of Schefer et al. (1994b) and others, clearly show the inclination of the flame base of a lifted flame, and the difference of liftoff height on both sides sometimes may be as large as a jet width. Obviously, evolution of flow modes other than the axisymmetry may play a role in the stabilization of the lifted flame.

Recently, the role of helical modes in the growth and evolution of jet flow and the effect of helical forcing on flow manipulation attract intensive studies and some remarkable results have been achieved. Corke et al. (1991) demonstrated the non-coexistence of the helical and axisymmetric modes and the resonant mode-selection phenomenon of the jet flow in the presence of feedback. Hussain (1986) pointed out that unlike the axisymmetric ring vortices helical structures have low dissipation and can be expected to be long-lived. The domains of large helicity and dissipation are spatially exclusive. For the generation of streamwise vortices, Lasheras et al. (1986) showed that the spanwise vorticity caused by positive and negative strains created by the spanwise vortices induces the formation of concentrated regions of streamwise vorticity on either side. Martin and Meiburg (1991 and 1992) used an inviscid vortex filament numerical technique to study the three-dimensional evolution of the jet subject to axisymmetric, azimuthal and helical perturbations. The emphasis was placed on the concentration of streamwise vorticity in the braid region and the formation of streamwise braid vortices induced by ring vortices under various perturbations. In their experiments Liepmann and Gharib (1992) verified that streamwise vorticity may evolve and be amplified in the braid region between the primary vortical structures. In a heated jet Monkewitz et al. (1989, 1990) showed the self-excitation and radial ejection of fluid into secondary side jets and proposed a side-jet generation mechanism. Brancher et al. (1994) improved Monkewitz's side-jet mechanism in their numerical simulation and demonstrated that the side jet is not directly linked to the deformation of the vortex rings but rather to the occurrence of coherent streamwise vortex pairs in the braid region. In a round jet, pairing usually causes both merger and expansion of the primary vortical rings and enhances the evolution of the secondary three-dimensional structures. What role does secondary three-dimensional structures, especially the streamwise vortices, play in the observed inclination of the lifted flame mentioned above? Also, how do the flow and the lifted flame respond to the external helical excitation of various modes? Investigation into these issues will enhance our understanding of the various stabilization characteristics in the flame base of a lifted flame. In addition, it will be helpful to achieve better control of the flame by manipulating excitation of various modes. These issues motivate the current study.

2 Experimental systems

The flame and cold flow experiments are carried out on a circular jet burner with a diameter of 1.0 cm, from which partially premixed propane-air mixture at an equivalence ratio of 8 emerges. The essential features of the experimental arrangement are shown schematically in Fig. 1. A noise reduction chamber, with convoluted foams lining the interior, is used to reduce the noise generated by the supply system. A honeycomb unit and five fine mesh screens are installed in the settling chamber to manage the flow quality. The jet nozzle wall is contoured with a fifth-order polynomial profile and has an area contraction ratio of 400. The fuel jet exit velocity is maintained at 7 m/s. At such a low velocity, quantitative measurement data and qualitative visualization images can be compared consistently with each other. The corresponding Reynolds number,

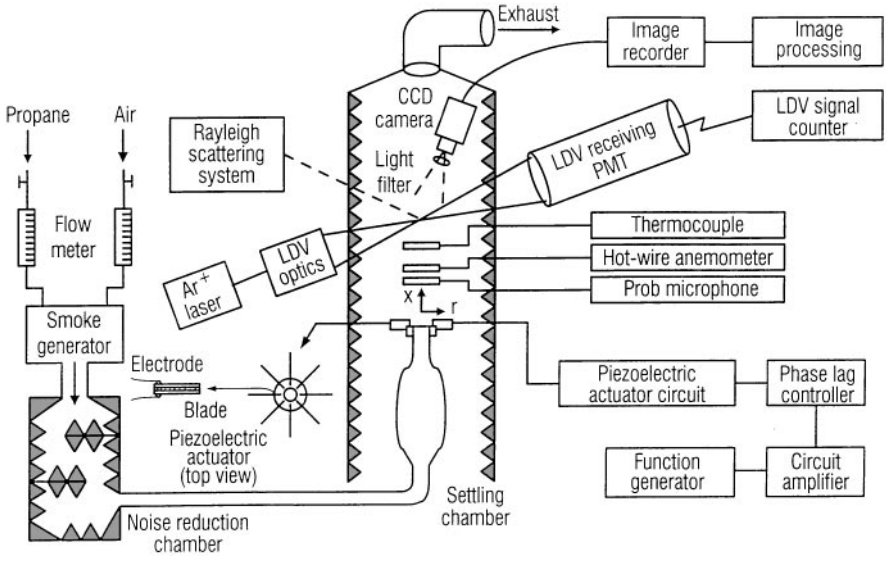

Fig. 1. Schematic diagram of the experimental system

based on the nozzle diameter and exit velocity, is 4700, and the fundamental frequency of the axisymmetric mode measured in the initial region of the jet flow is 330 Hz. With appropriate flow rectification the jet exit shows a top-hat velocity profile. The turbulence intensity is 0.25% in the unforced case, which is verified by both hot-wire and LDV measurements. In the present study, piezoelectric actuators are employed to introduce perturbation of various modes to the flow at the jet nozzle exit. A perturbation wave can usually be expressed in the exponential form, $p(x, r, \phi, t) = p_0(r) \exp[i(\alpha x - \beta t \pm m\phi)]$, where β is the frequency of the wave, α is a complex constant whose real part gives the wavenumber and the imaginary part determines the growth rate of the wave, and m is the azimuthal (helical) mode number. The initial turbulence levels of the excited jet flows measured in the centerline in the immediate downstream vicinity of the actuators ($X/D = 1.3$) are 0.4% in the axisymmetric forcing, 0.35% in the azimuthal forcing of $m = 1$ mode, and 0.32% in the $m = 2$ mode.

Conventionally, introduction of time-harmonic excitation with loud speakers at or near the jet exit has been an important tool to distinguish the individual instability mode in the broad disturbance spectrum in studies of instability characteristics of jet flows and stabilization of lifted jet flames. However, piezoelectric actuators are becoming an important substitute for loud speakers in many advanced areas of application. They are lightweight, miniature in size, easily conformed to the facility, robust in hazardous environment, and effective in generating the desired perturbation. They are also ideal for performing helical excitation on jet flows and flames. As shown in Fig. 1 eight piezoelectric actuators equally placed along the circumference of the nozzle exit are used to excite the jet flow. Each actuator is a composite of a thin (0.2 mm) blade, 10 mm wide and 19 mm long, partially sandwiched between two rectangular piezoelectric plates, as indicated by the magnified view in Fig. 1. Conducting electrodes are deposited on each of the piezoelectric plates. One end of the composite actuator is rigidly fixed to a base ring mounting on the nozzle exit so that approximately 70% of its length is cantilevered. When an electric field is applied across the electrodes, the actuator bends about the fixed end. The magnitude and direction of the displacement of the free end is nominally uniform and depends on the magnitude and polarity of the applied voltage. Also shown schematically in Fig. 1 is the driving circuit which includes a function generator, a high voltage amplifier and a phase-lag controller. This circuit is capable of generating either axisymmetric or helical excitations. The function generator generates the periodic wave of required frequency and amplitude with known initial phase angle. The phase-lag controller shifts the wave by a designated phase angle and the shifted voltage wave is applied to drive each piezoelectric actuator through the voltage amplifier. The maximum frequency response of the actuator is 10 kHz. The presence of these actuators has virtually no effect on the flow when they are not in use. This was verified by preliminary test results showing negligible variations of momentum thickness and turbulence intensity. The performance of the actuator system in generating the desired excitations is evaluated by using a pair of probe microphones (B & K 4182) placed in the immediate downstream vicinity of the actuators ($X/D = 1.3$) at the radial location of $r/D = 0.5$ of the jet without flow. Note that in the present experiments the actuators extend from the nozzle exit plane to the location of $X/D = 1.2$ in height.

Although microphones are widely used to measure pressure fluctuations in jet flows, for examples: Petersen (1978), Monkewitz et al. (1990) etc., they tend to create disturbance in the flow and their signals are easily contaminated by other sources. In the present study probe microphones are used to avoid these problems. The probe microphone (B & K 4182) is specially designed with a narrow rigid probe tube, 0.84 mm in diameter and 100 mm long, and an internal impedance matching tube inside the microphone housing. The high impedance of the narrow probe tip enables local measurements to be made within a volume as small as 1 cm^3 with high spatial resolution. The impedance matching tube reduces the effect of reflections within the probe tube by matching the impedance at the exit of the cavity in front of the microphone diaphragm. The size of the probe tube is small enough to have no effect on the major turbulent activity of the flow. Since most of the energy content in the velocity spectrum of the present flow is found to be below 1 kHz, with the mean velocity of 7 m/s the size of the smallest energy-carrying eddies is expected to be 7 mm, which is much larger than the probe diameter. Besides, the probe microphone is placed in the vicinity of the jet without intruding into the flow. To further justify the application of the probe microphone in the present flow a preliminary test is performed by simultaneously placing the probe microphone and a hotwire at $X/D = 2.5$ of the present jet flow excited at the fundamental frequency of the axisymmetric mode of 330 Hz. At this location the first pairing process of the axisymmetric mode dominates the flow. The spectral results in Fig. 2 clearly show that the structural characteristics of the fundamental, the subharmonic and the harmonic frequencies of 330, 165, 495 Hz, etc., are properly captured by the probe microphone as well as the hot-wire. Hot-wire rakes are usually employed for jet flow measurements. However, for the present purpose of helical mode measurements, it is very difficult to align the wire properly to the characteristic azimuthal motion

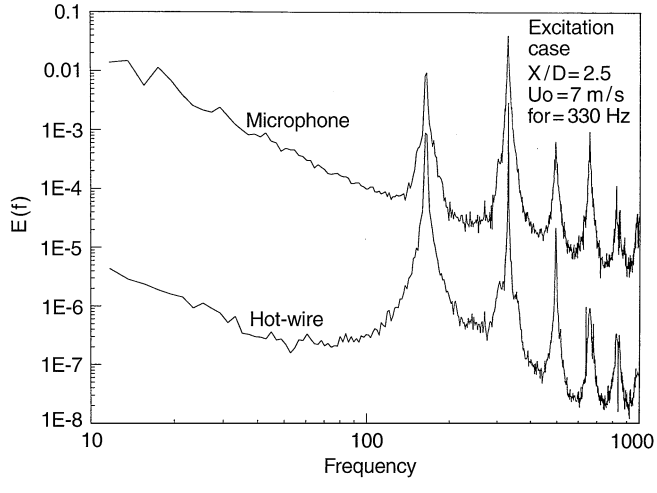

Fig. 2. Comparison of the spectral distributions of a jet flow excited at the fundamental frequency of the axisymmetric mode as measured by hot wire and probe microphone

of the helical mode even using the cross-wire because the motion is usually three-dimensional in nature. Besides, hot-wires are poor in directional resolution. The mode decomposition technique, as discussed in details by Michalke and Fuchs (1975) using correlation of pressure outputs of a pair of microphones, is adopted for analyzing the helical modes in the present study. One of the probe microphones is fixed at a point on an arbitrary reference axis, the other is moved along a horizontal circular arc at an increment of 10° from 30 to 180°. To avoid interference between microphone probes, measurement between 0 and 30° is skipped. This pair of probe microphones are used to verify the performance of the piezoelectric excitation system. By phase averaging, the normalized correlation of pressure outputs is plotted against azimuthal angle in Fig. 3. The solid line indicates the ideal profile of the $m=1$ helical forcing, and the square symbols are the corresponding measurement of actuator outputs. The averaged relative error is less than 2%. In addition, the circle symbols in Fig. 3 are the measured data of the axisymmetric forcing case, which are to be compared with the ideal actuator output of uniform amplitude profile. In general, the piezoelectric actuator has very good performance with only minor distortion due to the amplifier circuit and can meet the excitation requirements.

Laser sheet lighting through the jet flow seeded with smoke particles provides longitudinal and cross-sectional flow visualization images in the present study. The illuminating facility consists of a 3 W argon-ion laser and an optical lens module, including reflecting mirrors, a cylindrical lens and a focusing lens, which provides a light sheet of 0.8 mm thickness in the test region. For the present experiments, flow images are captured by a CCD camera (SONY DXC-750) and recorded on a professional recorder (SONY VO 9600) at 30 frames per second, through a frame code generator. The CCD camera is operated at a shuttle speed of 2000 s^{-1}. The coded images can later be retrieved accurately for analysis. The CCD camera has a total of 512×512 pixels in one frame and the light intensity in one pixel corresponds to the gas concentration in a small volume of 0.04 mm^3.

Other instruments employed in this study are thermocouples for temperature in the flame, an LDV system for determining velocity and turbulence characteristics and a laser Rayleigh scattering system for fuel-air premixture concentration measurement in the upstream unburned region of the lifted flame. Details of the LDV system can be found in a previous paper (Chao et al. 1991). The optical and signal processing modules of the laser Rayleigh scattering system and the justification of its application in the lifted flame were described in details in Chao et al. (1994).

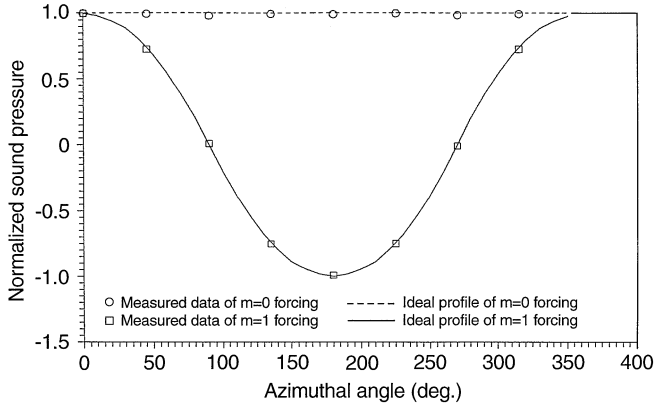

Fig. 3. Comparison of azimuthal variation of normalized sound pressure level from 8 actuators to ideal variation for axisymmetric (dashed) and helical (solid) modes

3 Results and discussions

3.1 Characteristics of the cold flow

As we use premixed propane and air, the fuel concentration in the jet is low relative to air. The maximum density ratio at the nozzle exit is less than 1.1 relative to ambient air. Therefore, the density effect is expected to be small, especially near the flame base of current interest in the near field of the jet where near stoichiometric mixture is expected. Besides, in the near field the vortex and flow characteristics are velocity-dominant and diffusion and density effects are less important. Side by side image comparison of vortex and flow characteristics in the cold flow and in regions upstream of the lifted flame base has been made and verified the above argument in Fig. 3 of a previous paper by Lin et al. (1993). From a detailed near field jet flow visualization (see, for example, Liepmann and Gharib 1992), the roll-up of the periodic axisymmetric vortices can be classified in the transverse views into the ring region of the vortex and the braid region between two successive vortices. In the unexcited air jet of the current study (not shown), the initial roll-up into an axisymmetric vortex is found around $X/D=3$. The structure appears to be axisymmetric before the end of the potential core at $X/D=6$, and becomes asymmetric behind $X/D=7$, associated with a zigzag motion. The axisymmetric vortices break down after the end of the potential core. In the far field, $X/D>7$, the jet is in a form of expanding spiral and the helical motion (azimuthal instability) becomes dominant. Helical excitation can be achieved by exciting the piezoelectric actuators with a prescribed phase difference between the adjacent actuators. As shown in Fig. 4 of the longitudinal and transverse views of the jet flow excited at the $m=1$ mode, the flow becomes azimuthally unstable in space near $X/D=2.5$ and secondary instabilities appear as fingers attached to the ring and the braid structures in the transverse views. These fingers may further grow into mushroom-type streamwise vortex pair, similar to the Bernal-Roshko structures in the mixing layer. These streamwise vortices first appear in the braid region (see also Liepmann and Gharib (1992) and Brancher et al. (1994)) and usually five to nine fingers (or lobes) are found in the flow image. In Fig. 4 when the $m=1$ azimuthal mode is amplified by external excitation, among the fingers in the transverse images one of them grows rapidly into a streamwise vortex as can clearly be seen in the longitudinal view and the ring structures become zigzag in pattern. This zigzag motion of the ring is directly associated with the helical perturbation and the multiple fingers may be related to the finite number of actuators. For the case of a helical perturbation only, Martin and Meiburg (1992) in their numerical simulation found that concentrated structures do

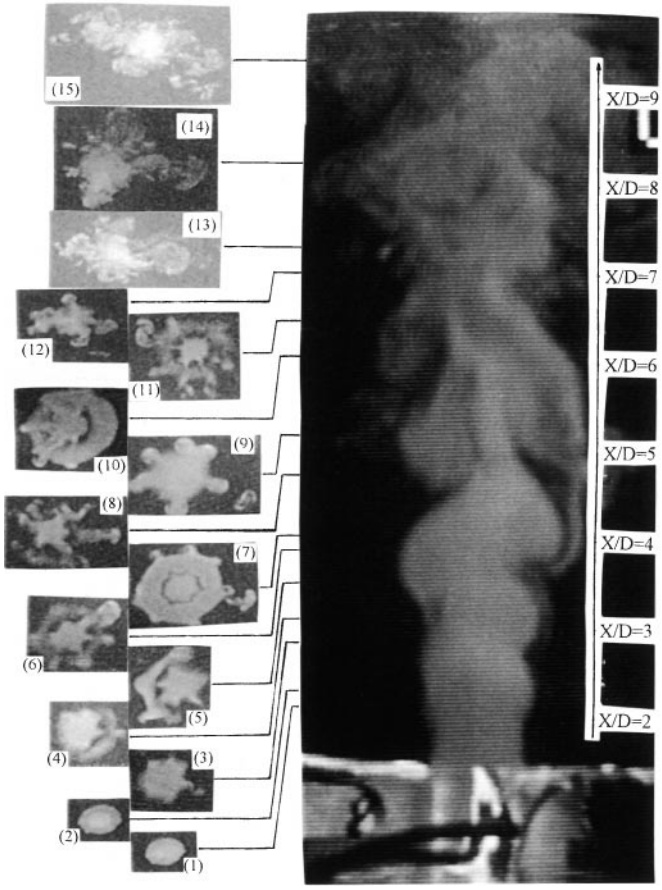

Fig. 4. Structural evolution of $m=1$ excited jet in longitudinal and transverse views

not form in the braid. However, by introducing an additional periodic azimuthal perturbation, they observed emergence of concentrated streamwise braid vortices all of the same sign in contrast to the counter rotating braid vortices of ring-dominated jets. Our current cold flow results are consistent with their numerical predictions. The excitation generated by the current piezoelectric actuators can be considered as a superposition of a helical perturbation and a periodic azimuthal perturbation. However, they did not show the stronger streamwise vortex under $m=1$ forcing. In their simulation using inviscid vortex filament, they have to terminate the computation after a certain time. With increasing time the braid vorticity is being resolved less and less well. They suspected that viscosity which is absent in their simulation might become increasingly important in the real flow (Martin and Meiburg 1991). They can not proceed their computation long enough to reveal the complicated growth process of the stronger streamwise vortex in their inviscid simulation. At locations downstream of the end of the potential core, $X/D>7$, the jet looks much less orderly and the transverse view shows that the jet area becomes much larger and the primary ring structure is destroyed. Large streamwise vortical structures become dominant. To further compare the strength of the various instability modes at a certain location in the flow, the energy contained in different wave-modes can be decomposed using a cross-correlation technique, see Michalke and Fuchs (1975) and Jong (1995) for

Table 1. Natural case

X/D \ Mode(m)	0	1	2	3	4	5	6	7	8
2	0.83	0.09	0.02	0.01	0.01	0.01	0.01	0.01	0.01
4	0.67	0.19	0.03	0.015	0.01	0.04	0.01	0.04	0.01
6	0.44	0.37	0.05	0.03	0.03	0.04	0.02	0.04	0.02
7	0.29	0.43	0.07	0.04	0.03	0.06	0.03	0.05	0.01
8	0.18	0.48	0.08	0.06	0.06	0.08	0.03	0.08	0.02
9	0.09	0.49	0.12	0.05	0.03	0.09	0.03	0.09	0.04
10	0.05	0.49	0.12	0.04	0.03	0.12	0.03	0.1	0.02
11	0.02	0.45	0.12	0.06	0.03	0.15	0.03	0.01	0.02

Table 2. Forcing f_1

X/D \ Mode(m)	0	1	2	3	4	5	6	7	8
2	0.51	0.41	0.02	0.01	0.01	0.01	0.01	0.01	0.01
4	0.4	0.45	0.04	0.015	0.01	0.045	0.01	0.05	0.01
6	0.28	0.52	0.035	0.02	0.015	0.045	0.02	0.04	0.02
7	0.16	0.57	0.05	0.035	0.03	0.05	0.03	0.05	0.035
8	0.1	0.57	0.07	0.04	0.03	0.08	0.03	0.07	0.03
9	0.04	0.55	0.09	0.04	0.03	0.09	0.03	0.08	0.03
10	0.02	0.54	0.1	0.04	0.03	0.12	0.03	0.1	0.02
11	0.02	0.46	0.11	0.05	0.03	0.15	0.03	0.13	0.02

detailed decomposition procedure. The results of mode decomposition using the pressure signals from a pair of probe microphones are shown in Tables 1 and 2 for the natural (unforced) and the $m=1$ excited cases. The distribution of mode fraction for the natural case in Table 1 clearly indicates that the axisymmetric, $m=0$, mode dominates in the near field ($X/D\leqslant 6$) and the $m=1$ mode becomes dominant in the far field ($X/D\geqslant 7$). For the $m=1$ excitation case in Table 2 the $m=1$ mode is greatly enhanced in the near field and becomes dominant as early as $X/D=4$. Comparing with the unforced case, one can easily find out that the axisymmetric $m=0$ mode is also suppressed in the near field as evidenced by the drop in the mode fraction from 0.83 and 0.67 to 0.51 and 0.4 for the first two locations ($X/D=2$ and 4) respectively. The higher modes of $m=5$ and 7 are also intensified early in the flow as noted in the form of fingers in the transverse images in Fig. 4.

One of the important parameters concerning the stabilization of a lifted flame is the upstream premixing of the jet. The mass entrainment by the axisymmetric ring and asymmetric helical vortices is the major contribution to the upstream premixing and affects the flame stabilization. The global air volume entrained upstream of the flame base can be estimated by calculating the integrated volume flux from the LDV velocity data. The integrated volume flux, Q, at a fixed axial location can be defined by

$$Q=\int_0^{2\pi}\int_0^{R_{0.05}} U(r,\phi)\, r\, \mathrm{d}r\, \mathrm{d}\phi$$

where $U(r,\phi)$ is the axial velocity distribution at an axial location measured by the laser Doppler velocimetry, and

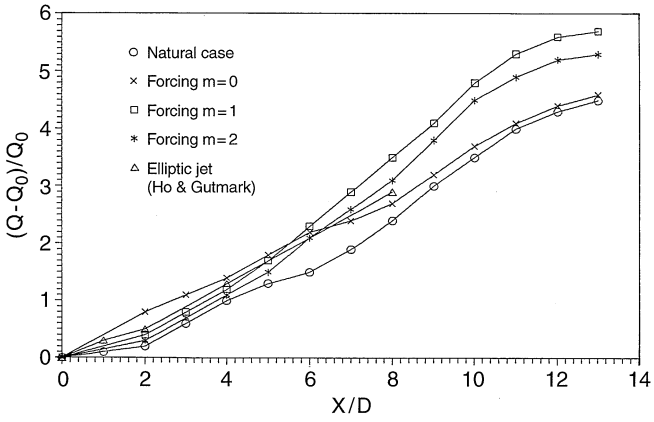

Fig. 5. Axial variation of the volume entrainment ratio with and without excitation

$R_{0.05}$ denotes the radius corresponding to $U/U_0 = 0.05$. The integrated volumetric entrainment, $Q - Q_0$, normalized by the nozzle exit condition $Q_0 = \frac{1}{4}(\pi D^2 U_0)$, for the unforced, $m = 0$ (axisymmetric), and $m = 1$, 2 (helical) forcing cases is plotted in Fig. 5. Comparing to the natural case, as expected axisymmetric forcing at the fundamental frequency, f_0, enhances entrainment even from the nozzle exit in the near field. Entrainment due to helical forcing at frequencies of f_1 and f_2 of the $m = 1$ and 2 modes, though is not so active initially, becomes significant around $X/D = 4$ and 5 as can be seen from the slope of the curves of helical forcing cases in Fig. 5 and $m = 1$ forcing has the largest overall entrainment after $X/D = 5.4$. The entrainment of $m = 2$ forcing is very similar to the case of the 2:1 elliptic jet reported by Ho and Gutmark (1987). The helical excitation leads to an increase in the cross-stream spreading of the jet shear layer. For mixing and combustion applications, non-circular jets typically entrain more ambient fluid than round jets having the same exit area and linear momentum flux. Therefore, similar to non-circular jets helical excitation may enhance jet flame stabilization through enhanced entrainment and mixing. The error in the current entrainment estimation is mainly due to the accuracy in LDV velocity measurement, which is estimated to be 3% in a previous paper (Chao et al. 1991), and the finite cutoff of radius in integration $R_{0.05}$, which is estimated to be very small for the current well-rectified jet flow. The density effect discussed above is also expected to be small for the current partially premixed case and its effect becomes even smaller due to entrainment. Though entrainment is important, the parameter directly affect the flame stabilization is the fuel–air premixing in terms of concentration or local equivalence ratio immediately upstream of the flame base which can be measured by Rayleigh scattering or other laser optical methods.

3.2
Lifted flame stabilization under helical excitation

In addition to the various phenomenological and theoretical models developed in the 80's mentioned above, recent studies on flame stretching (see for example Law 1988, Chen and Goss 1989, etc.), flame-vortex interaction (see Roberts et al. 1993, etc.), probability of premixedness (see Richards and Pitts 1991; Chao et al. 1994) and the recent concept of stabilization via triple or tribrachial flames (see Dold 1988; Kioi et al. 1993; Ruetsch et al. 1995; Muñiz and Mungal 1997) have greatly improved our understanding of the stabilization of lifted flames. Combining results from these studies, the major parameters controlling the flame base stabilization should at least include, local temperature, strain rate, concentration or probability of premixedness, and mixture fraction gradient in the stabilization zone. In turbulent flow the triple flame can stabilize itself by adjusting its structure to the local velocity field where the vortices are present. One may call this contorted flame leading-edge flame rather than triple flame, indicating a forward premixed region followed by a trailing diffusive tail (Muñiz and Mungal 1997). The triple flame is harder to extinguish than the diffusion flamelet because complete extinction of both the premixed wings and the diffusive tail is necessary. In the study of premixed flame-vortex interaction, Roberts et al. (1993) suggested that quenching occurs when the products cool to approximately 1300 K. In other words, the stabilization zone in the lifted flame base must be maintained at a certain temperature. This implies that the temperature of the premixture must be raised to a certain high value, usually higher than the auto-ignition temperature of the mixture, before entering the flame base. On the other hand, the importance of having flammable premixture in the stabilization zone has been reported (Eickhoff et al. 1984; Richards and Pitts 1991; Chao et al. 1994). The F probability (or the probability of premixedness, see Richards and Pitts 1991; Chao et al. 1994) accounts for the probability of the presence of a premixture with concentration within the flammability limits. It contributes to the estimation of the fraction of the local combination heat release used to maintain the flame stabilization in the flame base. Flame extinction by flame stretch in velocity gradient has been extensively studied (see the review by Law 1988). High strain rate in terms of velocity gradients causing local flame quenching is observed in the flame-flow or flame-vortex interaction. Chen and Goss (1989) proposed that the extinction in the flame base of a lifted flame is due to excessive strain when local Karlovitz number exceeds a critical value. In the current lifted flame, the flame is stretched due to the interaction with both the axisymmetric and streamwise vortices.

Although lift-off flames are generally found to stabilize downstream of the end of the potential core, it is shown (Chao and Jeng 1992; Lin et al. 1993) that the lifted flame in the hysteresis region generally stabilizes near the pairing location of axisymmetric vortices in the near field. Visualization photographs in Figs. 6a–c show the transverse and longitudinal views of the flame/flow interaction at the flame base of a lifted jet in the hysteresis region when helically excited at $m = 1$ mode. The image in Fig. 6a was taken from an angle about 45° in inclination relative to the jet axis with the laser sheet passing through the flame base to show the transverse view of the vortical structure at the flame base. The transverse view (Fig. 6a) of the flame base, indicated by the green region, shows multiple lobes with a larger (stronger) one on the right side of the jet. The flame image in Fig. 6b shows that the flame base, light blue in color, is hollow with multiple legs extending into the upstream region and the flame base is inclined toward the right side. There is clearly a strong streamwise vortex, green in

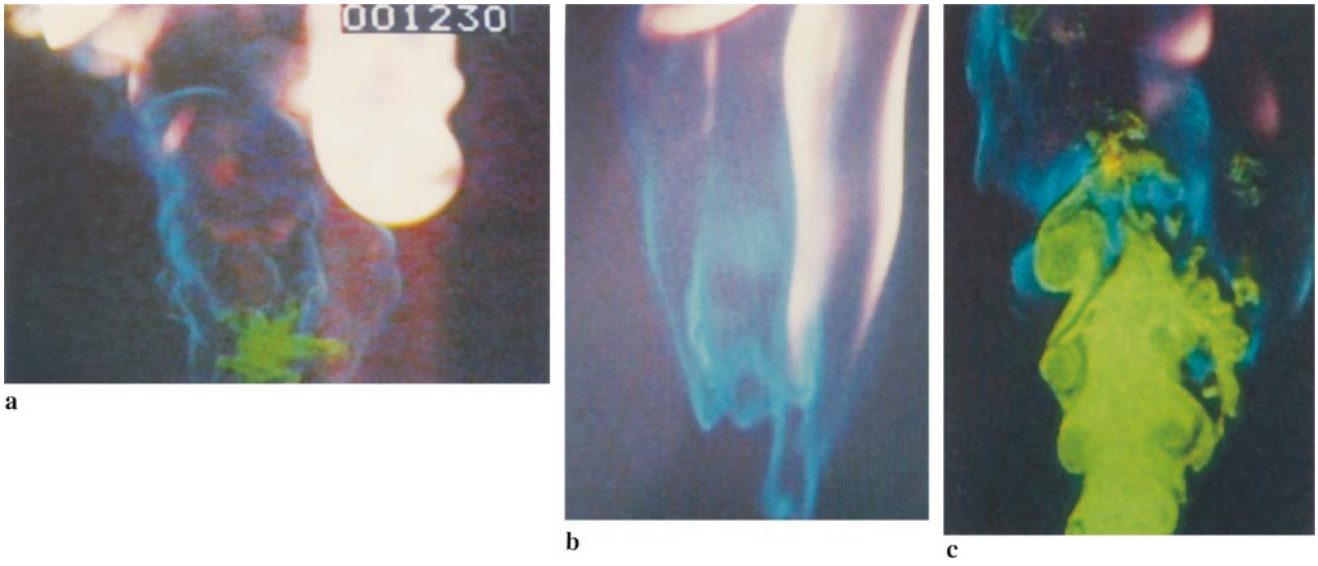

Fig. 6a–c. Effects of the $m=1$ helical excitation on the vortical structure of the jet flow and flame stabilization in the hysteresis region. **a** Transverse view of the lifted flame base, **b** the flame structure near the flame base, **c** longitudinal view of the flame-flow interaction at the flame base

color on the right side of the jet in Fig. 6c, extending upstream from the braid region between large ring vortices. This strong streamwise vortex with enhanced fuel-air premixing due to helical entrainment provides an additional convenient path for the lifted flame to propagate upstream so that the flame base on the right side extends farther upstream and the flame base is inclined. This result should be compared with that of axisymmetric forcing by Chao and Jeng (1992). When axisymmetrically excited the propagation of lifted jet flame is stopped by the pairing process initially and then the flame follows the "braid", which extends from the trailing edge of the paired vortex, to the next upcoming vortex (see Chao and Jeng 1992). This "braid" extending process can also be found on the left-hand side of the jet in Fig. 6c. In Fig. 6c, the surface of the streamwise vortex on the right is much more rugged than the "braid" on the left, indicating possible enhanced mixing. Furthermore, the streamwise vortex generally found in the periphery of the jet may extend farther upstream than the "braid". Since the enhanced mixing due to streamwise vortex and the flame destabilization due to aerodynamic strain play the major roles in the stabilization of the inclined flame base of the $m=1$ helically excited case, parameters related to these two processes are measured and delineated in the following. As for the enhanced entrainment and mixing, a 30–40% increase in entrainment as compared to the natural case is measured for cold flow when excited with the $m=1$ mode (see Fig. 5). Figure 7 shows the phase-averaged axial velocity contour (in m/s) at the location $X/D=5$ (near the lower flame base) at 0° relative phase angle as measured by LDV of the jet flow helically excited at $m=1$. At this relative phase angle and this location the stronger streamwise vortex (the stronger lobe) is found on the right side of the jet. In general, from the flow and flame visualization images one can find that the stronger streamwise vortex stays on the right side most of the time. In Fig. 7 the jet center is slightly shifted to the right corresponding to the zigzag pattern of the ring vortex of the $m=1$ case. The entrainment in each of the four quadrants can be estimated

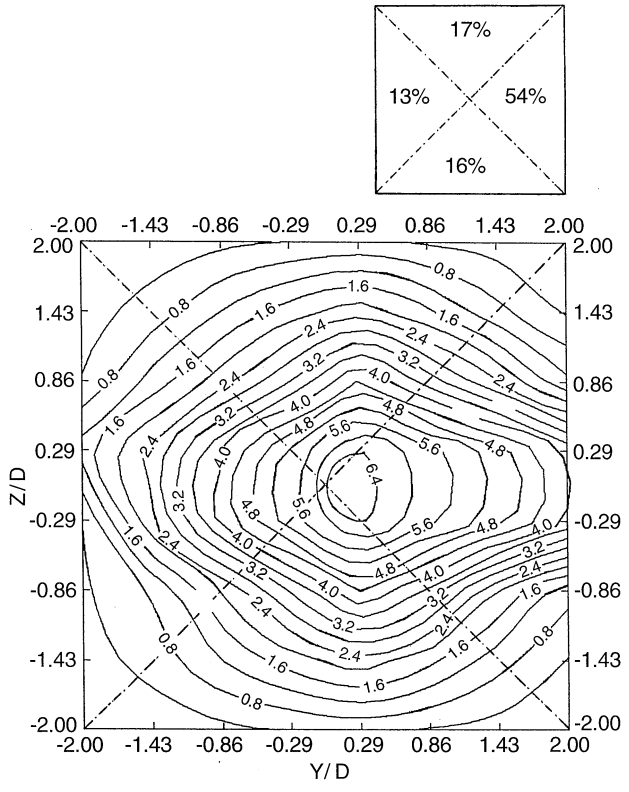

Fig. 7. The phase-averaged axial velocity contour of the jet flow helically excited at $m=1$ at a relative phase angle of zero degree at $X/D=5$ and the partition of the entrainment ratio in four quadrants

based on the velocity contour in comparison to that in the nozzle exit. More than 50% of the entrainment comes from the right quadrant see Fig. 7. To further account for the premixing at the flame base, the Rayleigh scattering system is employed to measure the fuel/air concentration at the inclined flame base of the helically excited jet flame of Fig. 6c. Figure 8 shows the

F probability (the probability of premixedness) and the strain rate at two axial locations corresponding to the flame base on the right ($X/D=5.0$) and the left ($X/D=5.7$) sides with the corresponding radial location of the streamwise vortex (abbreviated as "s.v.") indicated in the figure for reference. The F probability is obtained by statistically counting the percentage of time when the concentration of the fuel-air mixture from Rayleigh scattering data at the measurement location is within the flammability limits (see Chao et al. 1994). By carefully eliminating the background and compensating for laser power drifting in the experiment, the noise associated with the Rayleigh scattering system is dominated by electronic shot noise. The signal-to-noise ratio estimation and the Rayleigh system calibration against various propane-air mixtures of known mixture fraction were conducted and reported previously in Chao et al. (1994). The maximal deviation (the noise level) of the calibration data from the idealized linear calibration curve is less than 4% (Chao et al. 1994). The F probability is calculated based on 100 blocks of data with each block containing 1024 data points. Therefore the error in the F probability in Fig. 8 is negligible. In the jet flow the lifted flame may subject to aerodynamic stretch and even quench. The flame stretch comes from three major effects, i.e., aerodynamic straining, flame curvature, and flame motion (see Law 1988). Following Mueller et al. (1996) the stretch rate of the flame can be expressed as

$$K=\nabla\bullet\mathbf{v}-\mathbf{n}\bullet(\mathbf{n}\bullet\nabla)\mathbf{v}+S_L/R$$

where K is the stretch rate, S_L is the laminar burning velocity, $\mathbf{n}$ is the local unit normal to the flame surface, $1/R$ is twice the mean curvature of the local flame surface and $\mathbf{v}$ is the local velocity. The strain rate accounts for the aerodynamic effect of the flame stretch. It is the most important effect for the present case of lift-off flames in the hysteresis region where the flame stabilizes in the near field of large-scale vortical structures. The curvature effect of the flame stretch due to large-scale vortices is relatively small (see also Mueller et al. 1996). The strain rate is calculated from the axial and radial velocity data measured by LDV along the radial direction of the flame base of $X/D=5.0$ and 5.7. The small incremental distance along axial and radial directions at each position used for approximation of the strain rate differentiation is 0.50 mm. The tangential part of the strain rate was not measured due to the difficulty in laser beam accessibility. The tangential part is set equal to the radial component. The error introduced by this approximation is expected to be small as good correlation between two perpendicular velocity components in the plane of vortex rotation is obtained generally for large-scale vortices in the near field. The contribution of the tangential component is mainly due to the streamwise vortex in which the tangential and radial components have good correlation. The error in the velocity measurement using LDV has been discussed and calibrated previously (Chao et al. 1991). The accuracy of the present LDV measurements has been verified against the centerline velocity of a well-rectified jet flow in the initial region of the potential core. The maximum r.m.s. error is less than 3%. The spatial resolution is sufficient to enable the accurate computation of derivatives required to determine the strain rate. The error induced by the approximation of the tangential component using the correlated radial counterpart

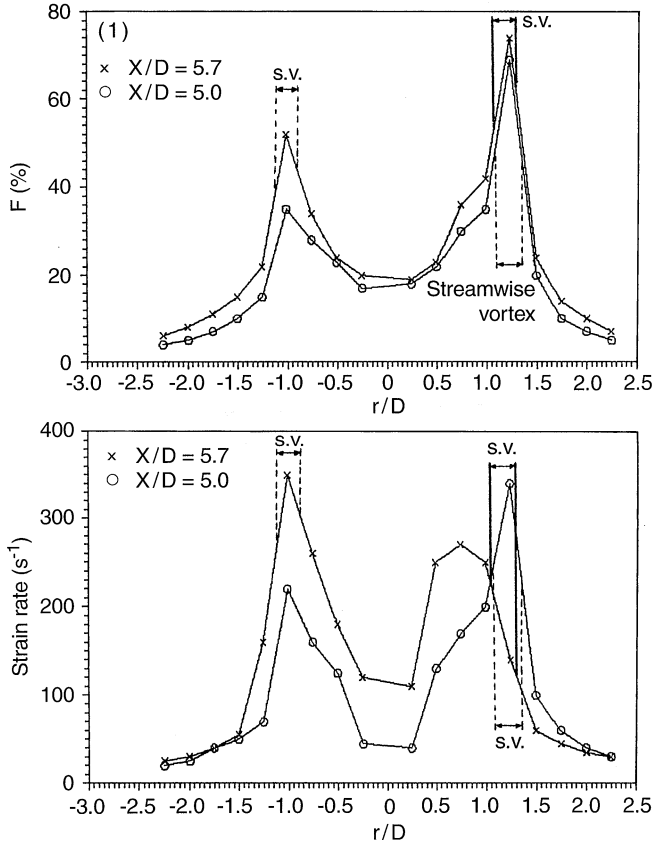

Fig. 8. The F probability and strain rate distributions of the jet excited at the $m=1$ helical mode at the two flame base locations $X/D=5.7$ and $X/D=5.0$ ("s.v." indicates the location of the streamwise vortex)

is estimated to be less than 10% in the near field of the current interest in this paper. In Fig. 8, the F probability of the streamwise vortex on the right side of the jet is above 60% at both axial locations. These high F probability regions coincide with the streamwise vortex. This result provides the evidence for the above conjecture that the streamwise vortex with enhanced fuel-air mixing provides a convenient flammable path for flame propagation. The strain rate on the right side of the jet at $X/D=5.7$ is below 230 s^{-1} and at $X/D=5.0$ is above 340 s^{-1} which is higher than the critical value (300 ~ 500 s^{-1}) for a propane lifted jet flame suggested by Chen and Goss (1989). This value is close to the strain rate at extinction for a counterflow laminar, propane–air flame of 400 s^{-1} as measured by Tsuji and Yamaoka (1969) but far below the stretch rate of 1600 s^{-1} for a premixed, stoichiometric counterflow propane-air flame measured by Law (1988). However, Fig. 14 of Law's review paper (1988) also shows that the extinction stretch rate decreases rapidly on both rich and lean sides of stoichiometric. The reason for these discrepancies is not pursued further in the current paper. Therefore with high F probability and low strain rate at $X/D=5.7$ the flame base there has a high probability to propagate along the highly premixed streamwise vortex upstream to $X/D=5.0$ and is quenched there by the high local strain rate. On the contrary, on the left side of the jet though the F probability is still high above 50% at $X/D=5.7$, yet the strain rate is higher than 350 s^{-1}. The flame base tends to be quenched at $X/D=5.7$, resulting in the phenomenon of "inclined flame base" in

Fig. 6(c). Similarly, the strain rate due to the azimuthal fingers (lobes) at the flame base is usually high and the flame surface is protruded and stretched. High strain rate associated with these fingers may cause flame extinction (or holes) at the flame base. This causes the "multiple-legs" phenomenon at flame base as seen in Fig. 6b.

As discussed above, aside from the parameters of concentration, F probability and stretch rate the matching of the local gas velocity with the local laminar flame velocity (or the local triple flame velocity) at the flame base is generally considered to be the stabilization mechanism of a lifted flame. Chao et al. (1992) showed that the upstream propagation of a lifted flame in the hysteresis region is usually prohibited by the cold entrainment of high velocity, much higher than the laminar flame velocity, after the vortex pairing process. Muñiz and Mungal (1997) demonstrated using PIV system that the local velocity at the instantaneous flame base is usually less than three times of the laminar flame velocity, thus verifying the possible triple flame in the lifted flame base. However, in their case the velocity concept is employed to delineate the stabilization of the lifted jet flame due to the axisymmetric ring vortices of the $m=0$ mode where the ring vortices induced from the Kelvin–Helmholtz instability are mainly due to the axial velocity difference. For the present cases of helical mode excitation and streamwise vortices, the axial velocity component is no longer dominant in the streamwise vortex and the entrainment process is different from the ring vortices. The stabilization of the lifted flame on the streamwise vortex is usually not simply due to the matching of the axial velocity at the flame base.

When the nozzle exit velocity is increased beyond the liftoff velocity, the flame tends to stabilize in the far field, usually downstream of the end of the jet potential core. Most of the near-field axisymmetric coherent vortices break down into smaller eddies as they pass through the tip of the potential core. Structures of helical modes and streamwise vortices as well as the less organized residues of the axisymmetric mode are the major large-scale objects in this region (see Dahm and Dimotakis 1990). The stabilization mechanism of a lifted flame in this region may quite different from that in the near field because the vortex structures in this region are much less organized and the entrainment due to vortices are less important. In other words, the influence of the vortices on flame stabilization is less significant as the vortical structures become less organized and the fuel stream becomes better premixed after a long evolution process through the near field. However, study of the stabilization process in this region is very difficult because the flame/flow interaction here is three-dimensional and unsteady. These features make experimental diagnostics, especially laser diagnostics which are mostly pointwise or planar, very difficult. The current results on the interaction of the lifted flame and the streamwise vortices of helical modes may shed light on the future study of the stabilization of lifted flames in the far field.

4
Conclusions

Experiments on the effects of helical excitation using piezoelectric actuators on the evolution of jet flow and the stabilization of lifted flame are performed. In addition to the common ring and braid structures, five or seven azimuthal fingers (or lobes) can be identified in the transverse images of the jet near field and when helically excited one of the fingers is enhanced and evolves into a strong streamwise vortex. The streamwise vortex generated in the braid region between the adjacent ring vortices play an important role in the flame stabilization mechanism. The streamwise vortex enhances the fuel-air mixing due to additional entrainment which provides an additional path for the upstream propagation of the lifted flame but the high strain rate associated with the streamwise vortex may destabilize the flame. The probability of premixedness (the F probability) and the strain rate are useful in analyzing flame stabilization. The inclined flame base and multiple-legs phenomena in the near field of the lifted jet flame are strongly associated with streamwise vortices and the fingers of the helical modes of the jet flow.

References

Brancher P; Chomaz JM; Huerre P (1994) Direct numerical simulation of round jets: vortex induction and side jets. Phys Fluids A6: 1768–1774

Broadwell JEE; Dahm WJA; Mungal MG (1984) Blowout of turbulent diffusion flames. Twentieth Symp (Int) on Combustion, pp 303–310. The Combustion Institute, Pittsburgh

Chao YC; Leu JH; Hung YF (1991) Downstream boundary effects on the spectal characteristics of a swirling flowfield. Exp Fluids 10: 341–348

Chao YC; Jeng MS (1992) Behavior of lifted jet flames under acoustic excitation. Twenty-fourth Symp (Int) on Combustion, pp 333–340. The Combustion Institute, Pittsburgh

Chao YC; Yuan T; Jong YC (1994) Measurements of the stabilization zone of a lifted jet flame under acoustic excitation. Exp Fluids 17: 381–389

Chen TH; Goss LP (1989) Flame lifting and flame/flow interactions of jet diffusion flames. AIAA paper no. 89-0156

Corke TC; Shakib F; Nagib HM (1991) Mode selection and resonant phase locking in unstable axisymmetric jets. J Fluid Mech 223: 253–311

Dahm WJA; Dimotakis PE (1990) Mixing at large Schmidt number in the self-similar far field of turbulent jets. J Fluid Mech 217: 299–330

Dold (1988) Flame propagation in a nonuniform mixture: the structure of anchored triple flames. Prog Astro & Aero AIAA 133: 240–248

Eickoff H; Lenze B; Leuckel W (1984) Experimental investigation on the stabilization mechanism of jet diffusion flames. Twentieth Symp (Int) on Combustion, pp 311–318. The Combustion Institute, Pittsburgh

Everest DA; Feikema DA; Driscoll JF (1996) Images of the strained flammable layer used to study the liftoff of turbulent jet flames. Twenty-sixth Symp (Int) on Comubstion, pp 129–136. The Combustion Institute, Pittsburgh

Gollahalli SR; Savaş Ö; Huang RF; Rodriquez Azara JLR (1986) Structure of attached and lifted gas jet flames in hysteresis region. Twenty-first Symp (Int) on Combustion, pp 1463–1469. The Combustion Institute, Pittsburgh

Ho CM; Huerre P (1984) Perturbed free shear layer. Ann Rev Fluid Mech 119: 443–474

Ho CM; Gutmark E (1987) Vortex induction and mass entrainment in a small-aspect-ratio elliptic jet. J Fluid Mech 179: 383–405

Hussain AKMF (1986) Coherent structures and turbulence. J Fluid Mech 173: 303–356

Jong YC (1995) The development of helical modes in a round jet and the effect on the stabilization of a lifted flame. PhD Thesis, National Cheng Kung University, Tainan, Taiwan

Kioni PN; Rogg B; Bray KN; Liñá n A (1993) Flame spread in laminar mixing layers: the triple flame. Combust Flame 95: 276–290

Lasheras JC; Cho JS; Maxworthy T (1986) On the origin and evolution of streamwise vortical structures in a plane, free shear layer. J Fluid Mech 172: 231–258

Law CK (1988) Dynamics of stretched flames. Twenty-second Symp (Int) on Combustion, pp 1381–1402. The Combustion Institute, Pittsburgh

Liepmann D; Gharib M (1992) The role of streamwise vorticity in the near-field entrainment of round jets. J Fluid Mech 245: 643–668

Lin CK; Jeng MS; Chao YC (1993) The stabilization mechanism of the lifted jet diffusion flame in the hysteresis region. Exp Fluids 14: 353–365

Martin JE; Meiburg E (1991) Numerical investigation of three-dimensionally evolving jets subject to axisymmetric and azimuthal Perturbations. J Fluid Mech 230: 271–318

Martin JE; Meiburg E (1992) Numerical investigation of three-dimensionally evolving jets under helical perturbations. J Fluid Mech 243: 457–487

Miake-Lye RC; Hammer JA (1988) Lifted turbulent jet flames: a stability criterion based on the jet large-scale structure. Twenty-second Symp (Int) on Combustion, pp 817–824. The Combustion Institute, Pittsburgh

Michalke A; Fuchs HV (1975) On turbulence noise of an axisymmetric shear flow: J Fluid Mech 70: 179–205

Monkewitz PA; Lehmann B; Barsikow B; Bechert DW (1989) The Spreading of self-excited hot jets by side jets. Phys Fluids A 1: 446–448

Monkewitz PA; Bechert DW; Barsikow B; Lehmann B (1990) Self-excited oscillations and mixing in a heated round jet. J Fluid Mech 213: 611–639

Mueller CJ; Driscoll JF; Reuss DL; Drake MC (1996) Effects of unsteady stretch on the strength of a freely propagating flame wrinkled by a vortex. Twenty-sixth Symp (Int) on Combustion, pp 347–355. The Combustion Institute, Pittsburgh

M*ü*ller CM; Breitbach H; Peters N (1994) Partially premixed turbulent flame propagation in jet flames. Twenty-fifth Symp (Intl) on Combustion, pp 1099–1016. The Combustion Institute, Pittsburgh

Mu*ñ*iz L; Mungal MG (1997) Instantaneous flame-stabilization velocities in lifted-jet diffusion flames. Combust Flame 111: 16–31

Peters N; Williams FA (1983) Liftoff characteristics of turbulent jet diffusion flames AIAA J 21: 423–429

Petersen RA (1978) Influence of wave dispersion on vortex pairing in a jet. J Fluid Mech 89: 469–495

Pitts WM (1990) Large-scale turbulent structures and the stabilization of lifted turbulent jet diffusion flames. Twenty-third Symp (Intl) on Combustion, pp 661–668. The Combustion Institute, Pittsburgh

Richards CD; Pitts WM (1991) An experimental study of the stabilization region of lifted turbulent jet diffusion flames. Fall technical meeting. Eastern section, pp 231–234, The Combustion Institute, Pittsburgh

Roberts WL; Drisccoll JF; Drake MC; Goss LP (1993) Images of quenching of a flame by a vortex-to quantify regimes of turbulent combustion. Combust Flame 94: 58–69

Ruetsch G; Verish L; Li*ñ*a′n A (1995) Effects of heat release on triple flames. Phys Fluids 7: 1447–1454

Schefer RW; Namazian M; Kelly J (1994a) Stabilization of lifted turbulent-jet falmes. Combust Flame 99: 75–86

Schefer RW; Namazian M; Filtopoulos EEJ; Kelly J (1994b) Temporal evolution of turbulence/chemistry interactions in lifted, turbulent-jet flames. Twenty-fifth Symp (Intl) on Combustion, pp 1223–1231. The Combustion Institute, Pittsburgh

Tsuji H; Yamaoka I (1969) The structure of counterflow diffusion flames in the forward stagnation region of a porous cylinder. Twelfth Symp (Intl) on Combustion, pp 997–1005. The Combustion Institute, Pittsburgh

Vanquickenborne L; van Tigglen A (1966) The stabilization mechanism of lifted diffusion flames. Combust Flame 10: 59–69